Slow-proton reemission from noble-gas solids

A. P. Mills, Jr., M. Leventhal, M. Y. Lanzerotti,* and D. M. Zuckerman
AT&T Bell Laboratories, Murray Hill, New Jersey 07974

E. M. Gullikson
Lawrence Berkeley Laboratory, Berkeley, California 94720

G. R. Brandes†
Brandeis University, Waltham, Massachusetts 02254-9110
(Received 14 February 1990)

A 1-μsec pulsed proton beam is being used to study H^+ thermalization and reemission from solid target surfaces in ultrahigh vacuum in order to help clarify analogous experiments using muon beams. Using a solid Ar target, vapor deposited on an $\approx$6-K Cu substrate, the reemission probability Y is 6×10^{-4} at a proton implantation energy $E_{H^+}=1.4$ keV and falls with increasing energy to 3×10^{-4} at $E_{H^+}=5$ keV and 2×10^{-4} at $E_{H^+}=15$ keV. Ne exhibits a 25% larger yield, while the yield for Kr is a factor of 4 lower. The reemitted protons are slow, with kinetic energies of order 1 eV. The reemitted proton yield Y decreases with an $\approx$100-m time constant, presumably due to deposition of neutral contaminants associated with the incoming beam, and thus ruling out the possibility that the slow protons originate from surface contaminants. For Ar, the observed variation of Y with E_{H^+} is interpreted with the help of a Monte Carlo calculation of the stopping and backscattering of the incident protons. The observed magnitude of Y is significantly greater than the calculated backscattering yield at the higher values of E_{H^+}. We therefore hypothesize that few-eV protons in the solid, which are considered "stopped" by the simulation, can diffuse a significant distance and escape into the vacuum. In our model, the diffusion length for few-eV protons in pristine solid Ar, λ_0, is found to be $\lambda_0=(50^{+70}_{-20})$ Å. However, the diffusion length we deduce from our measurements and simulations varies with E_{H^+}, possibly because of the interaction of the slow proton with its implantation trail. The vacancy density is computed to be too low for few-eV protons near the surface to be trapped at defects created by the energetic incoming particle. On the other hand, the proton neutralization probability could be dependent on the availability of free electrons in the ion trail of the implanted particle [O. E. Mogensen, J. Chem. Phys. **60**, 998 (1974)]. Extension of our model to the case of positive muons suggests that an experiment to moderate 4-MeV μ^+ with a solid Ar target [Harshman *et al.*, Phys. Rev. B **36**, 8850 (1987)] may have underestimated λ_0 for μ^+ due to sample impurities. It appears that the prospects for making a slow μ^+ beam are better than we thought, but that remoderation of a few-keV μ^+ beam using an Ar surface might have an efficiency less than 1% due to the high muonium-formation probability.

I. INTRODUCTION

The bombardment of solid surfaces with energetic positrons and positive muons is one method for producing slow beams of exotic particles. Beams of slow positrons, positronium, and positronium negative ions[1] have been known for many years. On the other hand, the more recently introduced slow muons,[2,3] thermal energy muonium,[4,5] and slow-muonium negative ions[2,6] are less common because muons are available in quantity only at a few accelerators. A promising way to produce slow muons is to bombard a solid rare-gas target with 4-MeV accelerator-produced muons and collect the small fraction ($\approx10^{-5}$) of the muons that emerge from the surface with only a few eV of kinetic energy.[3] While a more efficient source of slow muons might be the photoionization of thermal muonium,[7] a rare-gas target could prove to be a useful remoderator in a scheme to enhance the brightness of a muon beam:[8] Slow muons may be accelerated to a few tens of keV kinetic energy, focused to a spot much smaller than the primary moderator, and moderated again to near thermal energies using a second target surface. The process may be repeated until the spot size is microscopic, but it would only be useful if the losses were small. It is therefore essential to discover whether muon moderation by a solid rare-gas target has an efficiency of order unity when the muon energy is a few keV.

The few slow-muon experiments have left us with many questions about how muons and muonium atoms are emitted from solid surfaces. In particular, we do not know whether the slow μ^+ emitted from a solid rare-gas surface can be explained as a backscattering effect, or whether the diffusion of few-eV-energy μ^+ is also involved. To the extent that muons behave like light protons, an experiment to study proton interactions with

solid surfaces may help us understand muons better. To this end we have constructed a pulsed (0–16)-keV-energy proton beam and measured the reemitted yield of slow protons from rare-gas targets. We have compared our measurements to computer simulations and find that our results may be understood only if we invoke a proton diffusion mechanism not included in the simulations. Since the diffusion length appears to be greater the higher the proton implantation energy, we hypothesize that there is a probability for proton neutralization that diminishes with increasing energy of the implanted protons.

II. EXPERIMENT

A. Apparatus

A schematic drawing of our apparatus is shown in Fig. 1. A Varian ion gun I and 135° bending magnet B from an old residual gas analyzer produces a mass-filtered beam of protons from electron bombardment of water vapor. The ion gun chamber can be floated above ground potential by a voltage V_A. The protons are accelerated by a grounded grid as they leave the ion gun chamber, pass through a differential pumping region with pressure $P_2 = 7\times10^{-7}$ torr, are skimmed by a 3.2-mm-diam differential pumping aperture A, and enter an ultrahigh vacuum target chamber with background pressure $P_1 \approx 1\times10^{-9}$ torr. The protons strike a solid rare-gas target vapor deposited on a copper target surface C that is the end of a liquid-helium transfer cold finger. The angle of incidence of the protons is 45°, as indicated in Fig. 1. Reemitted protons are collected by a lens L similar to that used in Ref. 9, except that we are not using a grid immediately next to the target surface. The collected protons drift through a shielded drift tube D and are detected by a spiraltron electron multiplier (SEM). The cone of the SEM is biased at -1500 V and the collector at $+1400$ V. The drift tube is biased below ground at a potential V_3; a grounded stainless-steel shield X reduces the effect of the stray electric field from the drift tube on the path of the incident proton beam. An $\approx$77-K Cu radiation shield S surrounding the target (C) allows the sample to reach a temperature of $\approx$6 K and, in the neighborhood of the target surface, reduces the ambient pressure and hence the deposition rate of contaminant background gases.

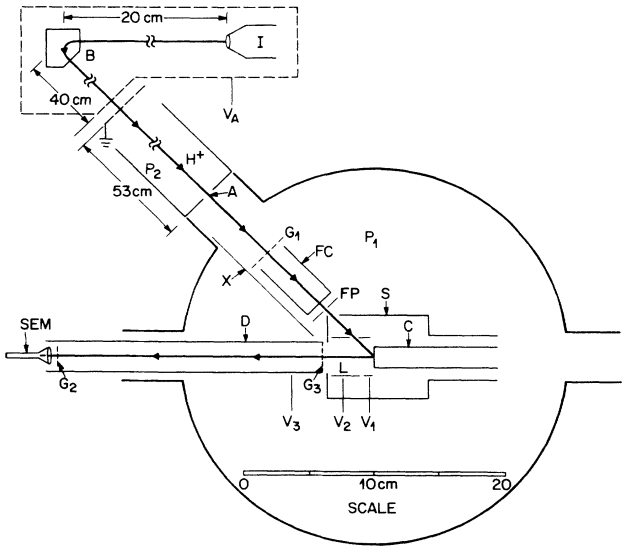

FIG. 1. Schematic drawing of the apparatus for producing a proton beam and measuring proton reemission from a solid-gas target surface. I, ion gun; B, bending magnet; V_A, acceleration potential; P_2, pressure in a differential pumping region; A, beam-defining aperture; FC, Faraday cup; G_1, grid to repel positive particles into the Faraday cup. The Faraday cup is withdrawn to allow the proton beam to strike the sample. FP, Faraday plate for determining that the beam is getting to the sample; S, cold shield surrounding the sample; C, copper cold finger target surface; L, ion lens; D, drift tube; SEM, electron multiplier; G_2, repeller grid; G_3, 90% transmitting drift tube grid; V_i, lens voltages.

B. Ion gun

The operation of the ion gun and mass filter is demonstrated in Fig. 2. For test purposes a mixture of water vapor and He gas (1.0×10^{-6} torr measured at the differential pumping stage P_2) was leaked into the chamber next to the ion gun I. The ion gun acceleration voltage was varied from 0 to 1000 V as the total beam current was measured using an electron multiplier mounted in place of the Faraday cup FC. The mass peaks that we have labeled He^+, H_2^+ and H^+ occur at acceleration voltages of 80, 165, and 330 V, respectively. The 1:2:4 voltage ratio and the absence of the 80-V peak when He gas is not used provide proof that the H^+ peak is correctly identified. The narrow width of the peak means that the H^+ beam will be uncontaminated by other species.

In order to measure the mass-to-charge ratio of the emitted ions by the time-of-flight method, we have pulsed

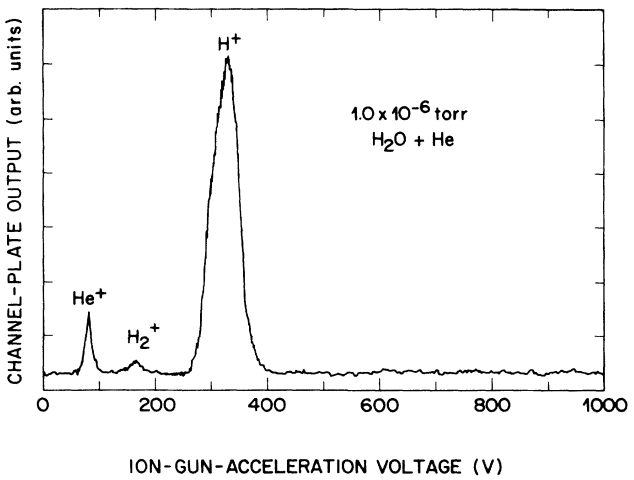

FIG. 2. Scan of ion-beam current vs ion gun acceleration voltage.

the proton beam. The ion gun acceleration voltage is set at a steady value of 250 V and raised periodically (23.3-kHz repetition rate) to 330 V using 80-V, 1.3-μsec-wide pulses. The time delay between the firing of the pulser and the detection of an event by the electron multiplier is recorded by a time-to-amplitude converter and multichannel analyzer. All the data reported here were obtained in runs lasting 100 sec.

The unpulsed proton-beam current, ranging from 3×10^{-13} A at $E_{H^+}=1.4$ keV to 9×10^{-13} A at 16 keV, is measured with an electrometer using the Faraday cup FC and a 90% transmitting grid G_1 that is biased 24 V positive with respect to the cup. Note that the attenuation due to G_3 is canceled in our measurements by the effect of the equally attenuating G_1. The charge per pulse of the pulsed beam is taken to be the unpulsed current times 1.3 μsec. The Faraday cup is drawn up out of the way to allow the proton beam to strike the target. In order to reach the target, the protons must pass through a 6.4-mm-diam hole in a Faraday plate FP, a 9.6-mm-diam hole in the Cu cold shield S, and a 6.4-mm-diam hole in the lens L. The latter two holes are drilled at a 45° angle relative to the axis of the lens. The beam elements are aligned with a HeNe laser, and the proton beam is tweaked for maximum intensity using small magnets on the chamber before the accelerator grids. Measurements of the current collected by the Faraday plate FP show that 99% of the beam reaches the target surface. The beam position was also observed using a channel electron multiplier array and phosphor screen to make sure that the incident beam was centered. The ambient magnetic field was reduced using a bucking coil so that the beam trajectory was independent of acceleration voltage. We also noticed that there was a neutral component in the beam that proved to be hydrogen atoms neutralized by collisions with the background gas in the 40-cm section following the bending magnet and before the acceleration grids.

C. Lens calculation

A drawing of the reemitted ion collection lens is shown in Fig. 3. In Fig. 4 we present the calculated[10] collection efficiency ϵ of the lens and detector as a function of particle emission energy E, assuming that the angular distribution upon emission is $\cos\theta\, d\Omega$. Neglecting the grid attenuation, the collection efficiency is unity for $E<E_0$, where E_0 is proportional to the product of the acceleration voltage V_3 times the area of the emitting surface; above E_0, the efficiency is inversely proportional to E:

$$\epsilon=\theta(E_0-E)+\theta(E-E_0)E_0/E\ . \tag{1}$$

Here, $\theta(x)$ is the Heaviside unit step function, $\theta(x)=\int_{-\infty}^{x}\delta(u)du$. At $V_3=-500$ V, we find from Fig. 4 that $E_0=0.3$ eV. In our calculations further on we will include the effects of the grids and the counting efficiency of the detector.

We have also calculated the deflection of the incoming proton beam due to the electric field of the lens, but neglecting the effect of the aperture in the lens. We find

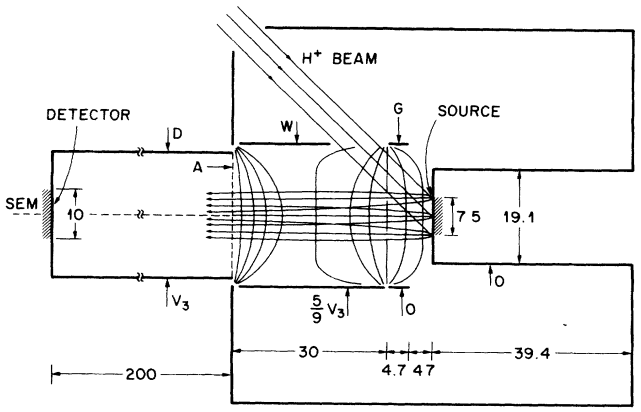

FIG. 3. Scale drawing of the reemitted ion immersion lens. The numbers are dimensions in mm. G, grid element; W, Wehnelt electrode; A, mesh anode; D, drift tube; SEM, spiraltron electron multiplier detector.

that the central ray is displaced from the center of the target (labeled "source" in Fig. 3) by

$$\Delta x=(1.25\text{ mm})(V_3/500\text{ V})(1.4\text{ keV})/E_{H^+})\ .$$

Compared to the diameter of the target illuminated by the full beam, Δx is negligible.

D. Sample preparation

To remove contaminants, the sample gas line and leak valve were baked at 150 °C for 24 h while being evacuated with a turbopump. The target chamber base pressure was $P_1=2\times10^{-10}$ torr when there was no water vapor being let into the ion gun chamber ($P_2=4\times10^{-8}$ torr). Under conditions just prior to vapor depositing a rare-gas sample layer, the ion pump was turned off, the target was at a temperature of approximately 6 K, the differential pumping chamber pressure was $P_2=7\times10^{-7}$ torr, and the target chamber pressure rose to 1.1×10^{-9} torr. The Faraday cup was left in the position for recording the ion current in order to intercept the straight-through gas

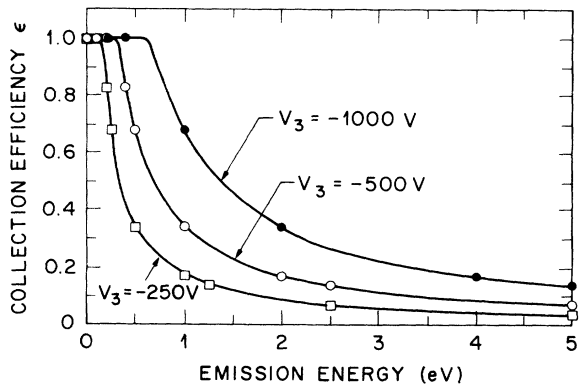

FIG. 4. Calculated collection efficiency of the immersion lens, drift tube, and detector of Fig. 3 for three values of the drift tube and lens voltage V_3.

from the differential pumping stage. The gas samples (99.999% pure) were admitted into the sample chamber at 1.5×10^{-5} torr for 60 sec. The ion gauge pressure reading must be multiplied by 0.713 for Ar gas, and the gas exposure in the target chamber per dose was consequently

$$Pt=(1.5\times10^{-5})(60)(0.713)=6.4\times10^{-4}\ \text{torr sec}\ .$$

The gas exposure inside the cold shield will be much less than outside because the pumping speed of the cold finger exceeds that of the holes through which gas may get inside the cold shield, and because the gas temperature inside is ≈77 K. In order to reduce the effects of background gas contamination of the surface, most of the data were obtained in pairs of 100-sec runs immediately following a gas deposition. Subsequently, the beam current was measured, and another dose of gas followed.

III. RESULTS

A. Preliminary measurements

A set of time-of-flight curves obtained with an Ar target bombarded by 6.5-keV protons is shown in Fig. 5 for three values of the lens voltage V_3. The peak that occurs at the smallest time following the voltage pulse to the ion gun moves to earlier times as the lens voltage is increased. The time of arrival of the incident protons at the target is found by plotting the time of the 65% point on the leading edge of the first pulse versus $V_3^{-1/2}$ and extrapolating to infinite V_3: We obtain the $t=0$ point shown by the arrow at 3.75 μsec. The slope of the t-versus-$V_3^{-1/2}$ line is

$$\alpha\equiv\Delta t/\Delta V_3^{-1/2}=0.55\pm0.07\ \mu\text{sec kV}^{1/2}\ .$$

Assuming there is a uniform electric field between the target surface and the drift tube grid G_3, the effective length from the target to the detector is $L_{\text{eff}}=28$ cm. The mass-to-charge ratio for the ions in the first peak is then

$$M/Q=2(\alpha/L_{\text{eff}})^2=0.72\pm0.18\ \text{GV}/c^2\ ,$$

in reasonable agreement with the 0.94 GV/c^2 expected for protons. It is therefore reasonable to assume that the first peak is due to H^+ ions.

The second earliest peak (labeled H^+! in Fig. 5) moves parallel to the H^+ peak, but is displaced by about 2.6 μsec. It appears to also be a H^+ peak, but its origin is the 330-eV neutral component of the incident proton beam. We shall see later that the low energy of the neutral beam means that it will not cause a significant amount of desorption into any higher mass peaks. Assuming that $M/Q=1$ for the first peak, the peaks with the longest time delays have values of M/Q that are approximately multiples of 28 and may tentatively be assigned to various ionization states of CO molecules and clusters.

Figure 6 shows the H^+ peak area per incident proton Y (see discussion below for how we compute Y), from Fig. 5 plotted versus lens voltage. Since Y diminishes by less than 10% and the peak shape is nearly constant as the lens voltage is decreased from $V_3=-1000$ to -250 V, most of the reemitted protons must have kinetic energies considerably less than 100 eV. Note that the sample surface is at ground potential and the SEM detector cone is biased at -1500 V so that the proton detection efficiency of the SEM is independent of V_3. In fact, conservation of brightness would lead to a detectable reduction in the area of the $V_3=-250$ V H^+ peak relative to the -1000-V peak if the perpendicular component of the reemitted proton energy were greater than $\frac{1}{4}$ eV. The dashed lines in Fig. 6 show the predicted change in the

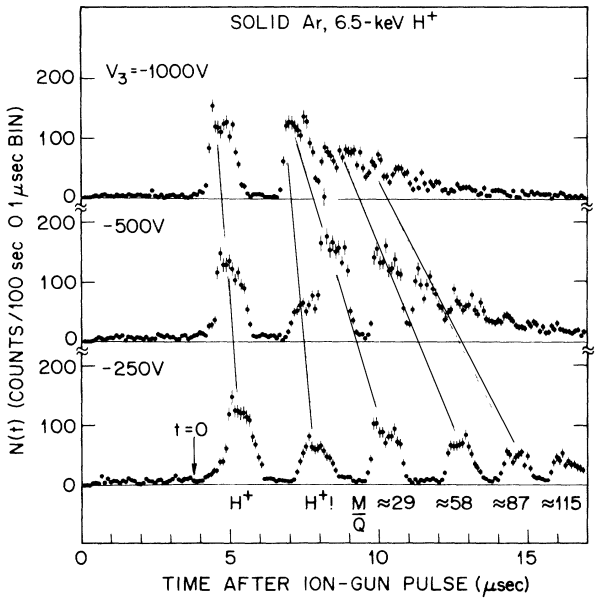

FIG. 5. Time-of-flight spectra for a solid Ar target bombarded by 6.5-keV protons. Data are shown for three values of the drift tube and lends voltage, $V_3=-1000$, -500, and -250 V. The three curves were obtained, respectively, 17, 15, and 19 m after the deposition of a solid Ar layer.

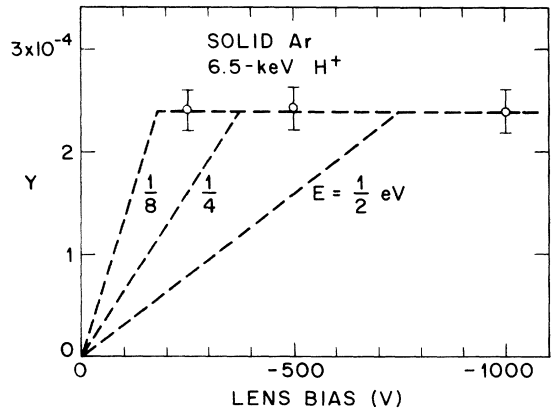

FIG. 6. Detected slow-proton yield vs lens bias. The lines show the calculated variation of yield assuming three different values of the emission energy.

measured Y for various emission energies using the collection efficiency from Eq. (1) and Fig. 4.

Before presenting our H^+ reemission yield data, we will summarize some further information we know about the "CO" peaks.

(1) The "CO" peaks are at the same M/Q in different rare gases (Fig. 7), although the intensity increases rapidly with decreasing atomic number of the rare-gas solid.

(2) The "CO" peaks grow with increasing primary proton-beam energy E_{H^+} (Fig. 8). The "CO" yield per incident proton is plotted versus E_{H^+} in Fig. 11, as discussed below.

(3) A bare, cold (6-K) Cu target exposed to the ambient vacuum (2.2×10^{-9} torr with the ion pump off) for 1 h shows little evidence for any "CO" peaks compared to an Ar surface under similar proton bombardment (Fig. 9). Apparently, the release of the "CO" ions requires the presence of the rare gas, perhaps because of an ionization mechanism involving excitons.[11]

(4) The absolute yield of "CO" ions per incident proton decreases with time (see Fig. 12 below).

One possible model that would be consistent with the above observations would be as follows.

(1) The "CO" peaks originate from the ionization of small quantities of "CO" molecules that happen to be at or near the surface. Carbon monoxide is a ubiquitous contaminant that, unlike water vapor, will have a substantial vapor pressure inside the 77-K cold shield.

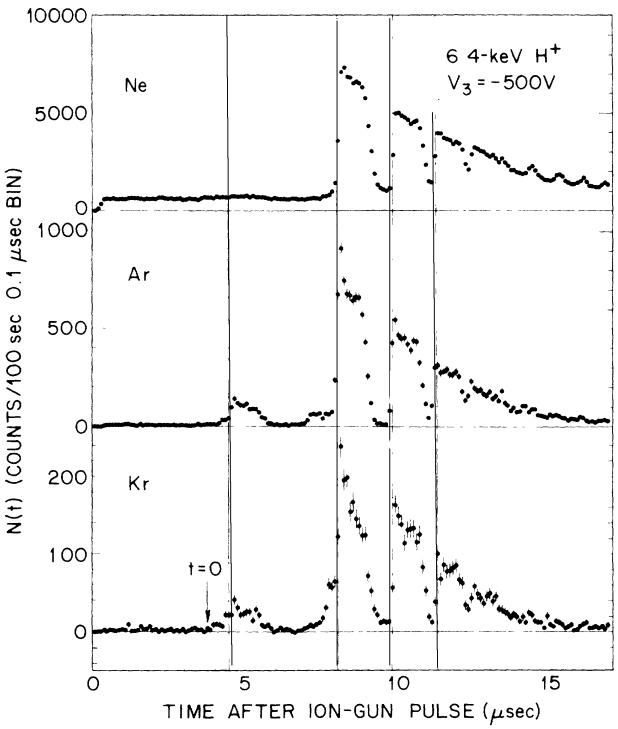

FIG. 7. Time-of-flight spectra for Kr, Ar, and Ne surfaces bombarded by 6.4-keV protons, showing that the delayed peaks are in the same positions for each gas surface. Note that the H^+ peak for Ne, although roughly equal in amplitude to the one from Ar, is difficult to see because it is small compared to the delayed peaks.

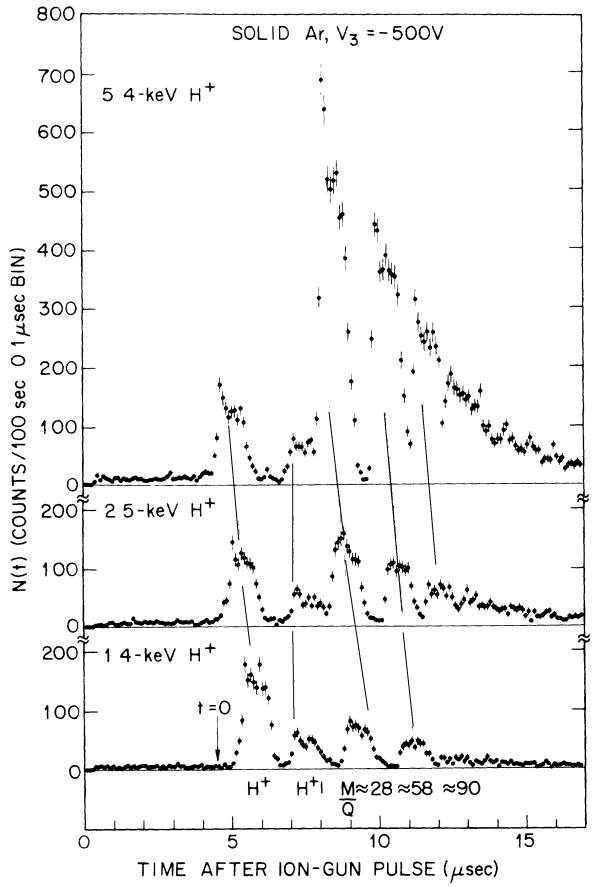

FIG. 8. Time-of-flight spectra for solid Ar showing that the delayed peaks grow with increasing proton-beam energy.

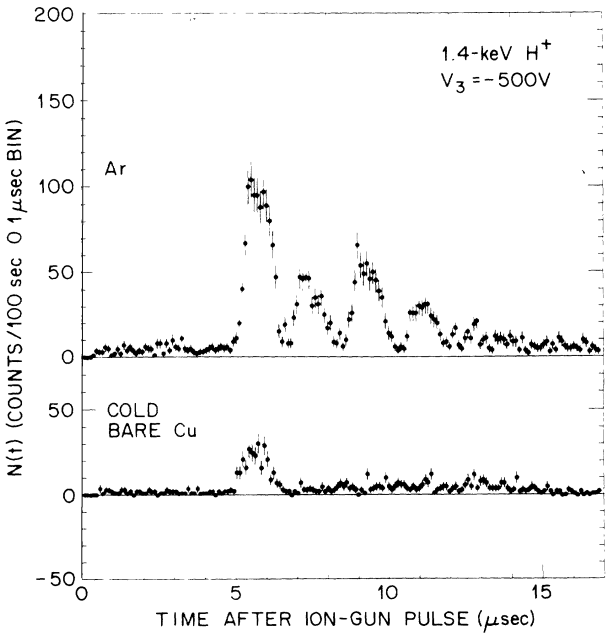

FIG. 9. Time-of-flight spectra demonstrating that a bare, cold copper surface exposed to the ambient vacuum for 1 h exhibits no delayed peaks like the Ar surface does.

(2) The CO at or near a rare-gas surface is ionized by excitons[11] that diffuse easily to the surface and are more abundant the higher the proton implantation energy.

(3) Absorption of a monolayer of line-of-sight water molecules from the ion-beam chambers reduces the "CO" yield by preventing CO^+ from diffusing into the vacuum. It is clear that experiments using samples deliberately doped with CO would be useful in testing our model.

B. Slow-proton-yield measurements

We have measured the yield of slow protons as a function of primary proton-beam energy by a series of measurements of which Fig. 8 is an example. The yield Y of slow protons per incident-beam proton is the area of the H^+ peak in counts per second times one elementary charge in coulombs, divided by the unpulsed-beam current in amperes, the duty factor of the pulsed beam, 0.0304, and the $(39\pm4)\%$ efficiency[12] of the spiraltron detector, including the 90% transmittance of the entrance grid G_2. As mentioned above, the attenuation due to G_1 and G_3 cancel each other in our calculations of the yield, since the one reduces the measured beam current, while the other reduces the detected current by the same amount. The results for solid Ne, Ar, and Kr and for warm Cu targets are presented in Fig. 10. The error flags represent the estimated $\pm10\%$ statistical uncertainties. The lines are monotonically decreasing freehand curves through the data. For comparison, Fig. 11 shows the "CO" yield per incident H^+ computed in the same way as the slow H^+ yield in Fig. 10. Since the "CO" peak grows while the H^+ peak diminishes with increasing E_{H^+}, the two peaks appear to have a different origin.

There is evidence shown in Fig. 12 that the slow-proton peak intensity diminishes with a $\approx$100-m time constant. All of the data in Fig. 10 were obtained in runs that started within 5 m of the end of the gas deposition. On the other hand, the "CO" $M/Q=28$ peak decreases with a $\approx$10-m time constant.

The slow-proton yield versus the number of Ar doses is displayed in Fig. 13. After a single dose we have two-thirds of the full yield. The thickness τ corresponding to a single does can thus be equated to roughly two slow H^+ diffusion lengths, if we assume that the slow-proton emission is entirely due to diffusion, and assume that the substrate surface acts like a sink for diffusing particles. We compute τ as follows. The rate of molecules hitting a surface is $\frac{1}{4}n\bar{v}$, where n is the number density of the gas, and

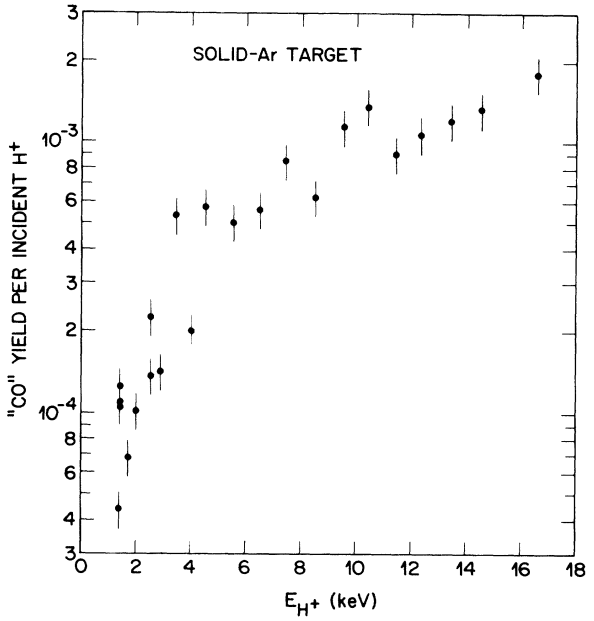

FIG. 11. Yield of $M/Q=28$ peak "CO" ions per incident fast-proton vs proton energy. The error flags are estimated $\pm15\%$ uncertainties in the individual yield determinations.

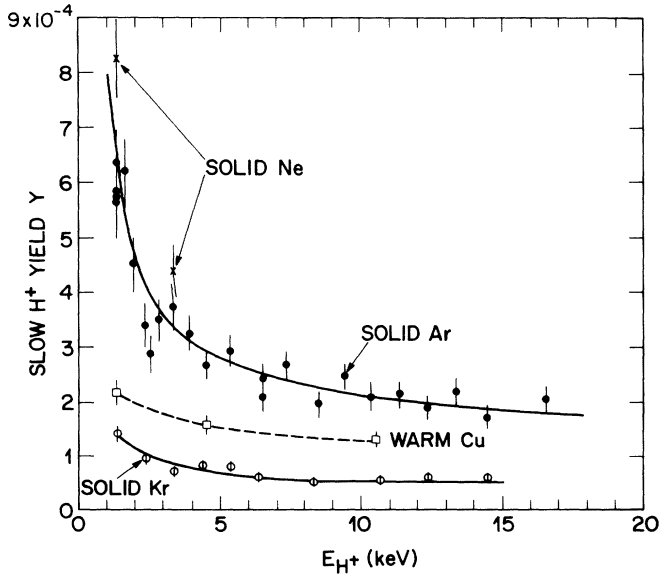

FIG. 10. Slow-proton reemission probability vs incident proton energy for solid Ne (×'s), Ar (solid circles), and Kr (open circles) and for a warm (300-K) copper surface (open squares). The error flags are estimated $\pm10\%$ uncertainties.

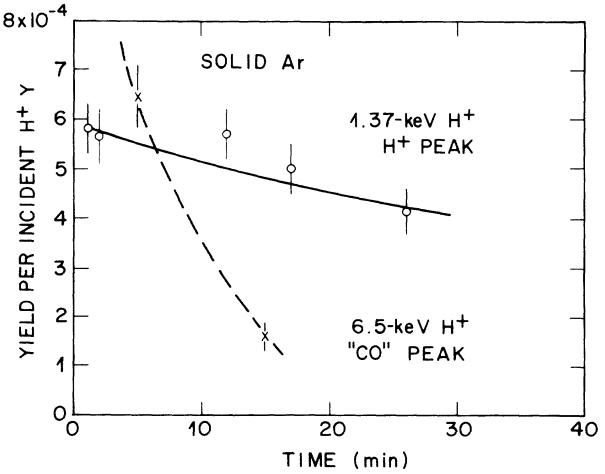

FIG. 12. Decrease of the slow-proton and CO yields with time after formation of an Ar sample surface.

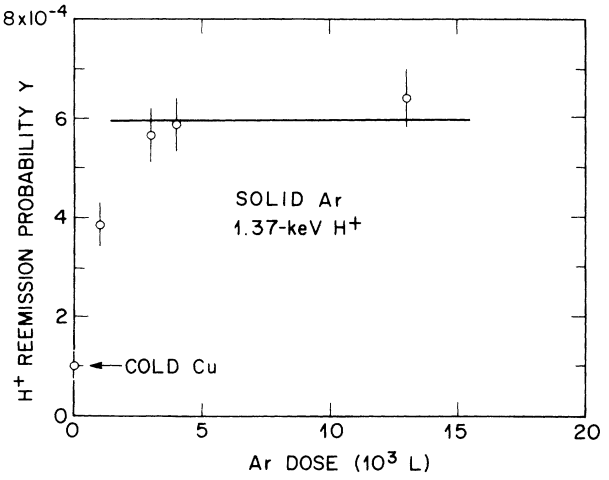

FIG. 13. Slow-proton reemission probability per 1.37-keV incident proton vs number of Ar doses. Data obtained at $E_{H^+}=6.5$ keV show that Y is (90±11)% of the thick target yield after two doses.

$\bar{v}$ is the average velocity of the gas molecules. The sticking coefficient[13] of Ar on solid Ar at 10 K is $q=0.95\pm0.05$. As mentioned above, the pumping speed of the cold finger (effective area $\equiv A_1=50\pm10$ cm^2) exceeds that of the holes (effective area $\equiv A_2=7\pm1$ cm^2) through which gas may get inside the cold shield. Consequently, the number density inside the shield is $n_{\text{inside}}=n_{\text{outside}}(A_2/A_1)$. The thickness is therefore

$$\tau=\tfrac{1}{4}n_{\text{inside}}\bar{v}tq\Omega$$
$$=\tfrac{1}{4}n_{\text{outside}}tq\Omega\frac{A_2}{A_1}\left[\frac{8}{\pi}\frac{kT}{M}\right]^{1/2}=(55\pm15)\ \text{Å}\ . \tag{2}$$

Here, t is the exposure time, $\Omega=3.98\times10^{-23}$ cm^3 is the volume per atom of the solid, and M is the mass of an Ar molecule. Note that

$$n_{\text{outside}}t=(Ptn_0/760\ \text{torr})(273/T_{\text{outside}})\ ,$$

where n_0 is Loschmidt's number ($n_0=2.69\times10^{19}$ molecules per cm^3 of an ideal gas at STP). In evaluating τ we have assumed a $T\approx77$ K temperature inside the cold shield, and we use $Pt=6.4\times10^{-4}$ torr sec obtained above.

IV. DISCUSSION

A. Proton emission model

We will now attempt to discover the origin of the slow H^+ emission observed in our experiment. One source of slow particles will be the low-energy tail of the distribution $N(E,\theta)$ of the backscattered protons. We have used a Monte Carlo computer code[14] to calculate $N(E,\theta)$. The backscattered protons have an angular distribution $\cos\theta\,d\Omega$, and a broad energy spectrum that generally decreases with emission energy E. The total number of back-scattered protons detected in our geometry for every incident energetic proton is

$$\delta=\int\epsilon N(E)dE\ , \tag{3}$$

where ϵ is taken from Eq. (1). The resulting values of δ for Ar are listed in Table I. The table also includes the values of Y for Ar read off the smooth curve for Ar in Fig. 10 at 1, 2, 5, 10, and 15 keV; the ±20% error assigned to the Y column includes our estimate of the calibration uncertainties.

The quantity δ is not negligible compared to Y. Nevertheless, our measurement cannot be explained totally in terms of a backscattering effect, not only because $\delta<Y$, but also because the data of Figs. 5 and 6 cannot be due to the partial collection of the broad backscattered energy distribution if it contributes more than about 25% of the count rate at $V_3=-500$ V, since Y could not then be independent of lens bias. Missing from the Monte Carlo

TABLE I. At five primary proton energies E_{H^+}, we have calculated the fraction δ of the incident protons that are backscattered and detected in our geometry, the yield Y of slow protons read off the smooth curve for Ar in Fig. 10, the exponent ν in the approximation ax^ν to the implantation profile for small values of the depth x [see Eq. (4)], the coefficient a, and the backscatter-corrected effective slow-proton diffusion length λ_{eff}. The error assignments for δ only account for the statistical errors associated with the Monte Carlo calculation. The ±20% error estimate for Y and the resulting error assignments for λ_{eff} include our estimates of both the statistical and calibration (systematic) errors.

E_{H^+} (keV)	δ (10^{-4})	Y (±20%) (10^{-4})	ν	a ($\nu=\frac{3}{4}$) (Å$^{-7/4}$)	$\lambda_{\text{eff}}=\left[\frac{Y-\delta}{\Gamma(\frac{7}{4})a}\right]^{4/7}$ (Å)
1	5.26±0.07	8.0	0.75	2.8×10^{-5}	$3.9^{+1.1}_{-1.6}$
2	3.04±0.14	4.5	0.84	1.04×10^{-5}	$4.8^{+1.5}_{-2.0}$
5	0.92±0.05	2.8	0.69	3.80×10^{-6}	$9.8^{+1.6}_{-1.8}$
10	0.40±0.01	2.1	0.79	1.39×10^{-6}	$16.4^{+2.1}_{-2.5}$
15	0.23±0.01	1.8	0.68	7.3×10^{-7}	$22.8^{+2.8}_{-3.1}$

simulation is the diffusion of few-eV protons in the solid rare gas. Particles that have "stopped" (i.e., slowed down to less than 10 eV) a few angstroms from the surface may still be able to escape from the solid. The fact that the slow-proton yield depends on Ar dose (Fig. 13) is also a good argument against the yield being due to backscattered protons and in favor of the model of diffusion of few-eV protons. In a diffusion model, the slow-proton yield per incident particle is

$$Y=\int_0^\infty P(x)\exp(-x/\lambda_{\rm eff})dx \ , \tag{4}$$

where $P(x)$ is the proton stopping profile in the rare-gas solid, and $\lambda_{\rm eff}$ is the effective mean depth from which a few-eV proton may diffuse to the surface. We have used the same Monte Carlo code[14] to calculate $P(x)$, and the results are displayed in Fig. 14 for primary proton energies $E_{H^+}=1$, 2, 5, 10, and 15 keV. We find that the "stopped" proton density in the first few hundred angstroms from the entrance surface increases approximately as a power of the depth x,

$$P(x)=ax^{\nu} \ , \tag{5}$$

with an average value of the exponent $\nu=0.75$ from Table I. The yield then becomes

$$Y=a\lambda_{\rm eff}^{\nu+1}\Gamma(\nu+1) \ , \tag{6}$$

where $\Gamma(x)$ is the gamma function, $\Gamma(x+1)=x\Gamma(x)$. The values of the coefficient a (computed assuming $\nu=\frac{3}{4}$) in units of $\text{Å}^{-(\nu+1)}$ are given at the five primary proton energies listed in Table I.

In order to separate the calculated effect of particle backscattering from our determination of $\lambda_{\rm eff}$, we have subtracted δ from our measured Y before solving for $\lambda_{\rm eff}$ using Eq. (6). In Table I we have computed the quantity

$$\lambda_{\rm eff}=\{(Y-\delta)/[a\Gamma(\nu+1)]\}^{(\nu+1)^{-1}} \ . \tag{7}$$

The error estimates for $\lambda_{\rm eff}$ are the result of propagating the ±20% overall error (statistical plus systematic) in Y. The results are plotted in Fig. 15 and show that $\lambda_{\rm eff}$ is a monotonically increasing function of E_{H^+}.

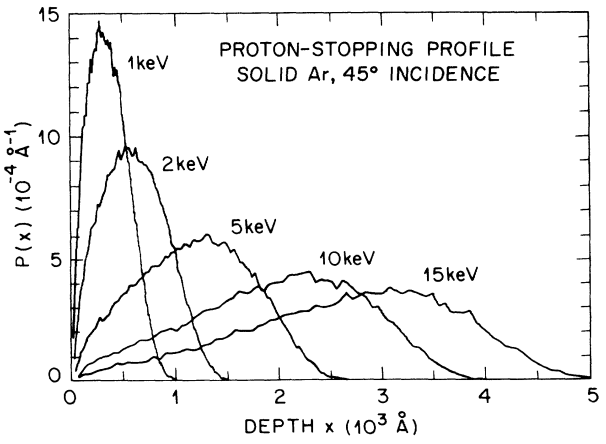

FIG. 14. Calculated stopping profiles for 1-, 2-, 5-, 10-, and 15-keV protons incident on a solid Ar target at 45° from normal.

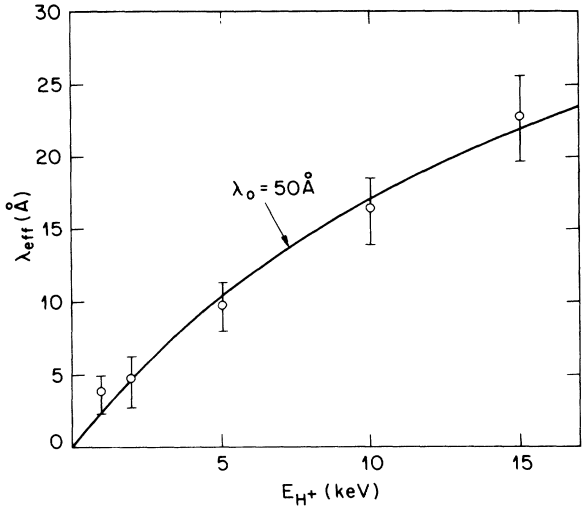

FIG. 15. Effective hot-proton diffusion length $\lambda_{\rm eff}$ computed from the data listed in Table I. The abscissa is the primary proton energy.

One might ordinarily think that the diffusion length would be independent of the implantation energy. The possibility that the efficiency of the lens and detector decreases at low energy because the reemitted protons have a higher kinetic energy or because of the deflection of the primary beam is contradicted by the data of Fig. 6. A second possibility is that the escape depth of a few-eV proton in pristine solid Ar is a constant λ_0 of order 50 Å, but that the yield is reduced because the implanted protons have some effect on the medium in which the protons are slowing down. There are too few defects produced per primary proton (we calculate that there are only about three vacancies produced per incident 5-keV proton) for trapping of the slow protons at their own defects to be a factor. On the other hand, electronic excitations or free electrons in the path of the proton could tend to neutralize it.[15] The effect might be less at higher implantation energies because the proton's path would be more dispersed. Although hot electrons can diffuse a comparatively long distance (10^3 Å) in the few psec it takes for a proton to stop, the ionization cloud near the surface might tend to produce neutral hydrogen atoms by analogy with the spur mechanism for positronium formation.[16] In the spur model, the ionization trail ("spur") of a positron can have a substantial influence on the probability for positronium formation. In many solids and liquids, the spur model gives a more satisfactory explanation of positronium formation than a description based on isolated charge pickup events.

Yet another possible reason for the nonconstancy of $\lambda_{\rm eff}$ could be that the Monte Carlo code is not very accurate at low energies where it has been least tested. For example, a systematic reduction of the quantities a and δ at low energies compared to high energies could conceivably yield a constant value of $\lambda_{\rm eff}$. At this time we have no way of testing such a possibility. For the purposes of making some predictions concerning muon remoderation,

we will take the Monte Carlo results at face value and assume that λ_{eff} is a quantity which is less than λ_0 due to an energy-dependent probability for neutralization. Since $\lambda_{\text{eff}} < \lambda_0$, Fig. 15 shows that $\lambda_0 > 20$ Å. In order to be able to extrapolate our proton results to muons, we parametrize the data in Fig. 15, using a form that makes λ_{eff} proportional to E_{H^+} at low energy and approach λ_0 at large energy:

$$\lambda_{\text{eff}} = (\lambda_0^{-1} + b^{-1} E_{H^+}^{-1})^{-1} . \quad (8)$$

The curve in Fig. 15 is a least-squares fit of Eq. (8) to the data. We find $\lambda_0 = 50^{+70}_{-20}$ Å and $b = 2.5^{+1.0}_{-0.5}$ Å keV^{-1} with a chisquare per degree of freedom $\chi^2/\nu = 1.07/3$. The value of λ_0 is to be compared with $\frac{1}{2}\tau = 27 \pm 8$ Å deduced from the variation of yield with Ar thickness in Fig. 13. (Remember that the factor $\frac{1}{2}$ is needed because we are assuming that the substrate is a sink for slow protons.) Since $\frac{1}{2}\tau$ was obtained from data taken at low E_{H^+} where $\lambda_{\text{eff}} \approx 5$ Å, but where roughly half the yield is from backscattering, the value for $\frac{1}{2}\tau$ does not seem to be in disagreement with the data of Fig. 15 and the fitted value of λ_0.

It is possible that the diffusion length varies less than suggested by Fig. 15, but that the yield is reduced by an energy-dependent neutralization that occurs prior to the diffusion regime. If f_+ is the probability for a proton near the surface to have escaped neutralization, we would have in this case[17] $\lambda_{\text{eff}} = \lambda_0 f_+^{(\nu+1)^{-1}}$.

In the spirit of the work of Thomas and Imel,[18] we may make a model for the neutralization by considering a classical process in which bare protons become neutralized at some rate due to a density n_x of excitons or free electrons. Since the protons are losing energy as they diffuse, their lifetime for escape from the solid is limited. We therefore describe the proton density n_H by a diffusion equation

$$\frac{\partial n_H}{\partial t} = D\nabla^2 n_H - \gamma n_H - \zeta n_H n_x , \quad (9)$$

where D is the diffusion coefficient, γ is an effective rate of protons falling below the escape energy, and ζ is the proton neutralization rate per unit concentration of excitons or bare electrons. Note that excitons diffuse hundreds of angstroms before becoming self-trapped in solid Ar.[11] As the protons slow down, the coefficients will be changing; for our purposes we will assume that they are constant so that we may solve Eq. (9) easily. Any values deduced for D, γ, and ζ will therefore be effective mean values. The yield is then given by Eqs. (4) and (6) except that we have an explicit expression for the effective diffusion length:

$$\lambda_{\text{eff}} = \left(\frac{D}{\gamma + \zeta n_x} \right)^{1/2} . \quad (10)$$

If we assume that the excitons or bare electrons become distributed over a volume equal to the cube of the proton range R, we have

$$n_x = (E_{H^+}/E_g) R^{-3} , \quad (11)$$

where E_g stands for the mean energy per electron-hole pair. Consequently,

$$\lambda_{\text{eff}} = (\lambda_0^{-2} + b^{-2} E_{H^+}^{-2})^{-1/2} , \quad (12)$$

where $b^{-2} = (\zeta/DE_g)(10 \text{ keV}/R_{10})^3$, where R_{10} is the mean depth for a 10-keV proton from Fig. 14, $R_{10} \approx 2300$ Å, and where we are using the approximate linearity of range with energy, $R \approx R_{10}(E_{H^+}/10 \text{ keV})$. Fitting Eq. (11) to the data of Fig. 15 yields $\lambda_0 = 30^{+22}_{-8}$ Å and $b = 2.2 \pm 0.4$ Å keV^{-1} with $\chi^2/\nu = 1.61/3$. The crude classical diffusion model therefore predicts a behavior similar to the *ad hoc* Eq. (8), with similar values of λ_0 and b.

B. Extrapolation to the case of muons

We will now attempt to scale our proton results to the case of muons. To estimate the muon diffusion length, we use the following approximations. Since positrons have a positive affinity $\phi_+ = 1.7 \pm 0.1$ eV for solid Ar,[19] protons and muons will also have positive affinities for solid Ar, differing by only a few tenths of an eV due to the difference in zero-point energy. Thus the energies below which H^+ and μ^+ cannot escape from solid Ar will be nearly the same. Furthermore, the inelastic threshold energies will be much the same for protons and muons. At energies less than the threshold for energy loss due to electronic excitations, the energy loss will be due solely to elastic collisions, and the energy loss per collision will be proportional to the mass of the proton or muon. We are assuming here that the energy losses are large compared to phonon energies so that phonon effects can be neglected. The energy gap in solid Ar is $E_g = 14.16$ eV. The true inelastic threshold is E_g less the binding energy of hydrogen in solid Ar, $E_b \approx 12$ eV, or about 2 eV. The relevant threshold for our problem could be a somewhat higher energy that includes the effects of the velocity dependence of the charge exchange and electron-hole pair creation cross sections. Since the cross section for scattering will probably be the same for eV protons and muons, a muon will suffer m_p/m_μ times more collisions on the average than a proton before it cannot escape from the solid. The diffusion length λ_0 will therefore be $(m_p/m_\mu)^{1/2} \approx 3\times$ longer for muons, $\lambda_0^\mu \approx 3\lambda_0^p$.

An estimate for the muon stopping profile may be made as follows. At a given primary particle velocity less than αc, the stopping power dE/dx will be the same for protons and muons and proportional to the velocity. Here, c is the speed of light, and $\alpha \approx \frac{1}{137}$ is the fine structure constant. At a given energy less than $\alpha^2 m_p c^2$, dE/dx for muons will be $\sqrt{m_p/m_\mu} \approx 3$ times greater than a proton's and the range one-third as much. Thus a of Eq. (5) should be $3^{\nu+1}$ times greater for μ^+, if we ignore the effect of the greater straggling for muons.

A scaling of the effects leading to the apparent implantation energy dependence of λ_{eff} is essentially impossible given our present state of ignorance. At low energies, we do know that the ionization density for a muon will be 3 times that of a proton of equal energy. Our model where $b \propto R^{3/2}$ would predict $b^\mu = 3^{-3/2} b^p$. Since muons pro-

duce much less radiation damage, defect trapping will be even less important for muons.

Summarizing, we have the predictions $\lambda_0^\mu = 3\lambda_0^p$, $a^\mu = 3^{\nu+1}a^p$, and $b^\mu \approx 3^{-3/2}b^p$. Below atomic velocities, or $E_\mu < 5$ keV, the slow-muon yield should be less than the slow-proton yield if the neutralization model has any validity. Similarly, above 10 keV where we might guess that $\lambda_{\rm eff}^\mu \approx \lambda_0^\mu \approx 150$ Å, the slow-μ^+ yield would probably be less than 1%. It is clear that an experiment to measure the reemission yield of 1–10-keV muons would immediately tell us much about the reasons for the apparent nonconstancy of $\lambda_{\rm eff}$ in Fig. 15.

The hot-positron diffusion length in solid Ar may be estimated from a measurement of the positron implantation energy $E_{1/2}$ at which the slow-positron yield falls to one-half of the yield extrapolated to zero energy,[20] $E_{1/2} \approx 7.2$ keV. The mean implantation depth[21] of 7-keV positrons is 8×10^{-5} g cm^{-2}, and the density is 1.65 g cm^{-3}. Thus, for positrons, $\lambda_0 = 5000$ Å, somewhat larger than the 2000 Å we would obtain by scaling our estimated $\lambda_0 = 50$ Å for protons by the inverse square root of the mass ratio. However, we note that a comparison with the scaled positron measurement may not make sense because positrons lose energy to phonons, not to individual particle collisions, as do protons.

Although one might object that a muon diffusion length $\lambda_0 \approx 150$ Å is 3 times larger than that estimated in Ref. 3, it is important to note that λ_0 should in fact be much longer in the higher-quality solid Ar of the present experiment.[22] An important implication is that the efficiency of a carefully prepared solid Ar primary muon moderator should be significantly better than reported in Ref. 3. It is obvious that further experiments using beams of other hydrogen isotopes such as muons and deuterons would be useful in clarifying the nature of the diffusion observed in our study.

V. CONCLUSION

We have observed slow-proton reemission from solid rare-gas surfaces and demonstrated that the effect for solid Ar is not dominated by the backscattering of the implanted protons. We have attempted to explain our results in terms of hot-proton diffusion and emission, and to make qualitative predictions concerning analogous experiments using positive muons. A theory of how eV-energy protons diffuse and become neutralized in a rare-gas solid would allow us to make a better connection between our results and the muon experiments. It appears that the prospects for making a slow-μ^+ beam are better than we previously thought, but that the remoderation efficiency for 10-keV μ^+ using an Ar surface might be less than 1%.

ACKNOWLEDGMENTS

We would like to thank Walter Brown, Len Feldman, and John Tully for helpful conversations. The work of E.M. Gullikson was supported by the U.S. Department of Energy under Contract Nos. DE-AC03-76SF00098 and SAN CID 9501, Task I. The work of G. R. Brandes was supported in part by the National Science Foundation (Grant No. DMR-8519524).

---

*Present address: Cornell University, Ithaca, NY 14853.

†Present address: AT&T Bell Laboratories, Murray Hill, NJ 07974.

[1]W. Cherry, Ph.D. dissertation, Princeton University, 1958 (unpublished); D. G. Costello, D. E. Groce, D. F. Herring, and J. W. McGowan, Phys. Rev. B **5**, 1433 (1972); for reviews, see A. P. Mills, Jr., in *Positron Solid State Physics,* edited by W. Brandt and A. Dupasquier (North-Holland, Amsterdam, 1983), p. 432; P. J. Schultz and K. G. Lynn, Rev. Mod. Phys. **60**, 701 (1988).

[2]D. R. Harshman *et al.,* Phys. Rev. Lett. **56**, 2850 (1986).

[3]D. R. Harshman *et al.,* Phys. Rev. B **36**, 8850 (1987).

[4]A. P. Mills, Jr., J. Imazato, S. Saitoh, A. Uedono, Y. Kawashima, and K. Nagamine, Phys. Rev. Lett. **56**, 1463 (1986).

[5]G. A. Beer *et al.,* Phys. Rev. Lett. **57**, 671 (1986).

[6]Y. Kuang *et al.,* Phys. Rev. A **35**, 3172 (1987); **39**, 6109 (1989).

[7]K. Nagamine and A. P. Mills, Jr., Sci. Pap. Inst. Phys. Chem. Res. Jpn. **80**, 67 (1986).

[8]A. P. Mills, Jr., Appl. Phys. **22**, 273 (1980).

[9]A. P. Mills, Jr., Rev. Sci. Instrum. **58**, 146 (1987).

[10]SLAC Trajectory Program, W. B. Hermannsfeldt, Report No. SLAC-226, 1978 (unpublished).

[11]C. T. Riemann, R. E. Johnson, and W. L. Brown, Phys. Rev. Lett. **53**, 600 (1984).

[12]From Fig. 9 of A. Egidi, R. Marconero, G. Pizzella, and F. Sperli, Rev. Sci. Instrum. **40**, 88 (1969), we read $\epsilon = (35\pm7)\%$ for 1.5-keV protons; from Fig. 2 of G. E. Iglesias and J. O. McGarity, Rev. Sci. Instrum. **42**, 1728 (1971), we read $\epsilon = (47\pm5)\%$ for 1.5-keV protons. The weighted mean of the two values is $(43\pm4)\%$.

[13]D. Menzel, private communication via John Tully.

[14]J. P. Biersack and L. G. Haggmark, Nucl. Instrum. Methods **174**, 257 (1980). We thank J. F. Ziegler for providing us with the Monte Carlo program TRIM-89.

[15]We have in mind (see Ref. 16) that the proton is perturbed by excitations that it made while it was at higher energy. For the latest views about the velocity dependence of the charge of a swift particle in matter, see J. F. Ziegler, J. P. Biersack, and U. Littmark, *The Stopping and Range of Ions in Solids* (Pergamon, New York, 1985), Vol. 1, p. 74.

[16]O. E. Mogensen, J. Chem. Phys. **60**, 998 (1974); O. E. Mogensen, in *Positron Annihilation,* edited by P. G Coleman, S. C. Sharma, and L. M. Diana (North-Holland, Amsterdam, 1982), p. 763.

[17]R. F. Kiefl, J. B. Warren, G. M. Marshall, and C. J. Oram [J. Chem. Phys. **74**, 308 (1981)] report a muonium formation probability of $(91\pm9)\%$ for muons implanted into solid Ar at 77 K. It is not known whether the muonium yield would be significantly reduced at the 6-K temperature of the present experiment. In any case, a large neutral fraction would mean that the diffusion lengths λ_0 are really much bigger than we have estimated.

[18]J. Thomas and D. A. Imel, Phys. Rev. A **36**, 614 (1987).

[19]E. M. Gullikson and A. P. Mills, Jr., Phys. Rev. B **57**, 376 (1986).

[20]A. P. Mills, Jr., and E. M. Gullikson, Appl. Phys. Lett. **49**,

1121 (1986).
[21]A. P. Mills, Jr. and R. J. Wilson, Phys. Rev. A **26**, 490 (1982).
[22]There are several reasons for expecting that our Ar samples were better than those used in Ref. 3: The base pressure of the vacuum system reported in Ref. 3 was 25 times higher than ours; there was no cold shield used in Ref. 3; the slow muon yield depended on the deposition rate of the Ar, whereas we observe no such effect; and the data collection times were an order of magnitude longer in Ref. 3 than in the present work.